Barium adsorption on hydrogenated $Si(100)2 \times 1$ surfaces

1996 J. Phys.: Condens. Matter 8 8799

(http://iopscience.iop.org/0953-8984/8/45/015)

J. Phys.: Condens. Matter **8** (1996) 8799–8814. Printed in the UK

Barium adsorption on hydrogenated Si(100)2 × 1 surfaces

D S Vlachos and C A Papageorgopoulos

Department of Physics, University of Ionnina, PO Box 1186, GR-451 10 Ioannina, Greece

Received 9 May 1996, in final form 30 July 1996

Abstract. An experimental study of Ba and H adsorption on Si(100)2 × 1 by Auger electron spectroscopy, thermal desorption spectroscopy, low-energy electron diffraction, electron energy loss spectroscopy, and work function measurements has been made. Measurements of hydrogen adsorption on a clean silicon surface have been made mainly for reference purposes. H on Si forms two different states, known as monohydride state Si(100)2 × 1:H and dihydride state Si(100)1 × 1::2H. Preadsorption of H made the surface order more stable without changing the sticking coefficient of Ba on the Si surface. The results supported the double-layer (DL) model for the first Ba layer on the monohydrided Si surface. Ba adatoms up to $\Theta = 1$ ML on the dihydride phase were relaxed at symmetric and equivalent sites following the (1 × 1) symmetry of the restored Si surface. TDS measurements showed that during Ba adsorption on the monohydride phase some of the H atoms were removed from their initial adsorption sites, and a new H energy state was formed at 425 °C which was attributed to the weakening of the Si–H bond in the presence of Ba adatoms. When Ba deposition took place on the dihydride phase, two new H states were successively developed. The first state at 220 °C was attributed to BaH_2 formation, and the subsequent one to a complex Ba–H–Si compound near 680 °C. The presence of hydrogen caused a considerable delay of barium overlayer metallization, in contrast to the early metallization of alkali on hydrogenated surfaces.

1. Introduction

The coadsorption of hydrogen and metals on different substrates has been intensively studied in the past [1]. Besides the theoretical interest on the coadsorption species, these systems have many considerable technological applications such as heterogeneous catalysis, thermionic energy converters, microelectronics, and photocathodes [2–6].

Among the metal adsorbates great effort has been given to the alkali adsorption. Adsorption of alkali on most metallic and semiconducting substrates causes an initial decrease of the work function to a minimum value and a subsequent increase to a final plateau. This is characteristic of the work function variation versus alkali adsorbate coverage [7]. It has been shown that coadsorption of hydrogen affects the properties of alkali adsorbates and especially the work function [8–11]. Specifically, preadsorbed hydrogen causes (i) an increase of the initial slope of the work function curve, (ii) a shift of the minimum value to lower alkali coverage, and (iii) an increase of the final work function value. These effects have been explained by Papageorgopoulos [9]. According to the latter author the preadsorbed hydrogen atoms induce a displacement of the alkaline overlayer outwards. This displacement results in an increase of the initial electric dipole moment of the adatoms, and prevents the charge transfer from the alkaline overlayer to the substrate. The latter causes an early metallization of the alkali layer, thus resulting a shift of the work function minimum to lower coverage. This explanation is consistent with the theory of

0953-8984/96/458799+16$19.50

Muscat and Batra [12]. Excess of hydrogen on the surface may form hydrides with an ionic character. Specifically, coadsorption of alkali and hydrogen on metal substrates has given some evidences of surface alkali hydride [13–17]. In some cases, however, hydrogen interacts with both adsorbate and substrate, forming complex compounds [18].

The coadsorption of alkali and H on Si substrate has been widely studied in the past [8, 19–22]. Electron scattering has shown that K adsorption causes a displacement of H and weakening of the Si–H bond [19]. Auger electron spectroscopy (AES) and thermal desorption spectroscopy (TDS) measurements suggest that preadsorption of H does not affect the sticking coefficient of K adsorption on Si(100)2×1 [8]. Moreover the surface states of caesium and hydrogen coadsorption on silicon have been investigated by Souzis *et al* with UPS measurements [20]. The results of the latter work indicate that adsorption of atomic hydrogen on the caesiated silicon surface has little effect on the work function minimum, making this system valuable as a source for negative-hydrogen-ion production [23–25].

Barium adsorption on metals has been also used for the production of H^- [26, 27]. This alkaline earth metal gives a stable work function of 2.5 eV and has relatively high electron density, $2.44 \times 10^{-3}\ a_0^{-3}$. These two factors enhance the negative-hydrogen-ion yield, which is useful in nuclear fusion experiments [28, 29]. Furthermore alkaline earth metals form hydrides which are stable insulators with predominantly ionic metal–hydrogen bonding [30, 31]. This hydride formation can be considered as an example of a metal–insulator transition. In addition theoretical studies have appeared on the possibility of the superconducting transition in hydrides of alloys of alkaline earth metals with alkali metals [32, 33].

In this paper we study Ba and H coadsorption on Si(100)2×1 at room temperature by AES, TDS, low-energy electron diffraction (LEED), electron energy loss spectroscopy (EELS), and work function (WF) measurements. This work is a continuation of a recent investigation of Ba on Si(100)2×1 [34].

2. Experimental details

All experiments were performed in an ultrahigh-vacuum system with base pressure of the order of 10^{-8} Pa. The techniques used were AES, LEED, EELS, TDS, and relative WF measurements by the diode method.

The sample was a Si crystal with (100) orientation and a (2×1) reconstructed surface. Ar^+ ion bombardment was used for the crystal cleaning with $E = 2.6$ keV at $P = 1.33 \times 10^{-4}$ Pa for $t = 30$ min. After bombardment the sample was heated at 1000 °C by passing current through a 0.05 mm Ta strip uniformly pressed between the sample and a Ta foil case. The specimen temperature T was measured with an NiCr–NiAl thermocouple spot welded onto the case and calibrated by an infrared pyrometer in the 600–1100 °C temperature range. The specimen heating rate for TDS measurements was 13 K s^{-1}. The crystal was considered clean when the ratios C(272 eV)/Si(91 eV) and O(510 eV)/Si(91 eV) of Auger peak heights were less than 1%. The Ba deposition took place by evaporation from a commercial source (SAES Getters), while the H adsorption was carried out by exposing the surface at pressure 1.33×10^{-3} Pa of hydrogen through a bakeable leak valve. It is well known that molecular hydrogen is not reactive with the silicon surface. For this reason a W filament at high temperature was placed 2 cm away from the crystal for the dissociation of H_2 into atomic H. The determination of Ba coverage was performed by a correlation of the AES and LEED measurements as in previous work [34]. The absolute coverage of one monolayer (1 ML) of Ba was considered equal to the surface atomic density of Si(100), 6.8×10^{14} atoms cm^{-2}.

3. Results and discussion

3.1. Adsorption of hydrogen on clean Si(100)2 × 1

Although this system has been widely studied in the past, the mechanism of the hydrogen adsorption and desorption on silicon remains controversial. Many experimental studies have been done with a wide variety of surface science techniques [35–47]. In parallel, several theoretical works have proposed mechanisms and models on surface structure and bonding as well as on the kinetics of hydrogen desorption [48–55]. In spite of the large number of papers, it was necessary to investigate the hydrogen adsorption on our clean Si(100)2 × 1 sample mainly for reference purposes. The study took place with LEED, TDS, and relative WF measurements.

Exposure of clean Si(100)2 × 1 to less than 1200 L hydrogen caused a small increase in background without changing the (2 × 1) LEED pattern. Further hydrogen exposure gradually changed the (2 × 1) pattern into a (1 × 1) one. These two structures are well known as the monohydride and dihydride phase respectively [37]. In the monohydride phase Si(100)2 × 1:H each hydrogen atom is bound on one dangling bond per surface silicon atom, while in the dihydride phase Si(100)1 × 1::2H two hydrogen atoms are associated by a silicon atom occupying the two available dangling bonds.

Figure 1 shows the work function variation versus hydrogen exposure. The work function decreases as the hydrogen coverage increases up to the completion of the monohydride phase, forming a plateau at a constant value of about 0.40 ± 0.05 eV (the average of five experiments). This work function curve is quite similar to those published in previous papers [20, 39]. By adopting the asymmetric (ionic) dimer bond model [56], a charge transfer occurs between the two adjacent silicon atoms of the dimer. In this way an additional electric dipole moment appears on the surface, thus increasing the work function compared to an ideal Si(100)1 × 1 surface. Adsorption of atomic hydrogen on the reconstructed (2 × 1) surface gradually removes the asymmetry of the dimer bonds, thus decreasing the work function of the surface during the monohydride phase. A recent theoretical investigation trying to explain scanning tunnelling microscopy (STM) images supports the transformation of asymmetric dimer bonds into symmetric ones [52]. As the work function is constant at about 800 L, we assume that no other asymmetric dimers exist. This means that the monohydride phase is completed, giving on average a ratio of 1:1 between adsorbed hydrogen atoms and surface silicon atoms. During the transition, however, the two phases may coexist because the (2 × 1) pattern becomes more diffused before the appearance of (1 × 1) structure. This is confirmed by TDS measurements as we will see below.

Figure 2 shows TDS measurements for different hydrogen exposures on Si(100)2 × 1. As this figure shows, one single TD peak (β_1) appears from the early stages of the hydrogen adsorption at 510 °C. At about 500 L, a new peak (β_2) is developed at 390 °C. These two peaks have been documented previously [44, 45, 57, 58]. The high-temperature peak is attributed to the monohydride phase (SiH) and the lower-temperature one to the dihydride phase (SiH_2). The appearance of the β_2 peak occurs before the completion of the monohydride phase, because the height of β_1 peak continues to increase. This indicates the coexistence of the two phases before the completion of the Si(100)2 × 1:H phase. When the β_1 TD peak stops increasing, the monohydride phase is completely formed. Further hydrogen exposure induces the prevalence of dihydride phase, transforming the reconstructed (2 × 1) surface into (1 × 1).

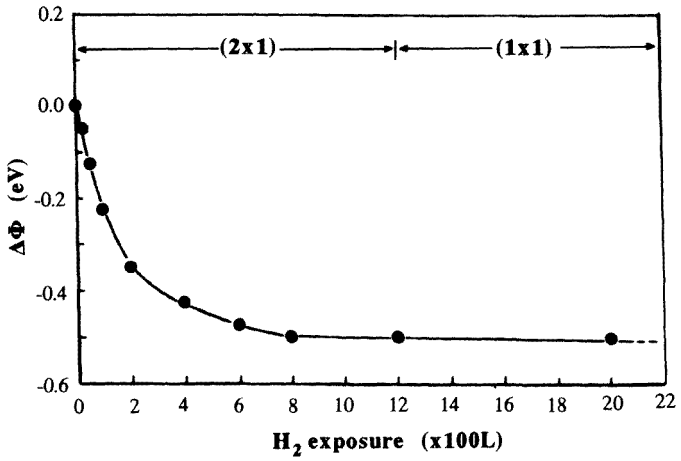

Figure 1. Work function variation $\Delta\Phi$ versus hydrogen exposure on clean Si(100)2 × 1. Surface structures observed by LEED are also shown.

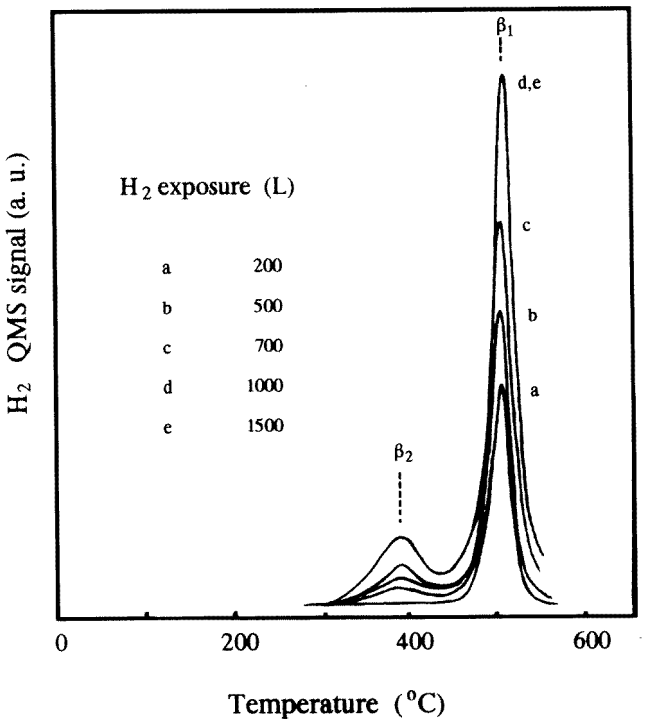

Figure 2. TD curves of H_2 at several exposures on clean Si(100)2 × 1.

The positions of the two hydrogen desorption peaks, correlated to the monohydride and dihydride phase, are independent of the surface coverage (figure 2). This is characteristic

of a first-order reaction. We can roughly calculate the activation energy for each case using the Redheads' equation [59]

$$E = RT_P\{\ln(\nu T_P/\beta) - 3.64\} \tag{1}$$

where T_P is the temperature of the TD peak, ν the preexponential frequency factor, and $\beta = 13$ K s^{-1} the heating rate of the specimen. setting $T_{P1} = 810$ K and $\nu_1 = 2 \times 10^{15}$ s^{-1} [60] in the above equation, we find $E_1 = 240$ kJ mol^{-1} or 2.49 eV/atom for the monohydride phase. This value is in good agreement with previous results [51, 53, 60]. In the same way, substituting $T_{P2} = 690$ K and $\nu_2 = 3 \times 10^{15}$ s^{-1} [60] in the Redhead equation, we calculate the desorption energy of dihydride species $E_2 = 206$ kJ mol^{-1} or 2.13 eV/atom. This value is equal to the one estimated by Gupta *et al* [44].

3.2. Ba adsorption on hydrogenated Si(100)2 × 1

Our next step was to study the adsorption of Ba on hydrogenated Si(100)2 × 1. Successive depositions of Ba, and subsequent annealing, gave the LEED patterns in table 1. As seen in this table, the Ba deposition above 1.5 ML, on both monohydride and dihydride phase, causes gradually the complete disappearance of the well ordered substrate structure. Similar disordering has been reported for Ba on clean Si, but it happened at substantially lower Ba coverage (0.5 ML) [34]. In the latter case Ba interacts strongly with the Si substrate from the early stage of Ba deposition. In the presence of H probably Ba, being bound with Si, interacts also partially with H on the dimer sites. This interaction prevents the destruction of substrate dimers for $\Theta < 1.5$ ML on the monohydride phase. Further Ba adsorption to 1.5 ML causes a high background, which is attributed to the disordering of the surface. Subsequent annealing, at relatively high temperatures, forms new ordered structures similar to those of Ba deposition on the clean Si(100)2 × 1 surface [34].

Table 1.

Ba coverage, Θ (ML)	Substrate	LEED pattern	T (°C)
$\leqslant 1.0$	Si(100)2 × 1:H	2 × 1	RT
< 1.5		2 × 1 (diffused)	
$\geqslant 1.5$		background	< 800
		2 × 4	800
		2 × 1	900
		2 × 3	1000
$\leqslant 1.0$	Si(100)1 × 1::2H	1 × 1	RT
< 1.5		1 × 1 (diffused)	
$\geqslant 1.5$		background	< 800
		2 × 4	800
		2 × 1	900
		2 × 3	1000

Each of these patterns corresponds to a certain barium coverage on silicon. There is no doubt that hydrogen is not involved in the phase transitions caused by annealing at $T \geqslant 800\,^{\circ}$C, because TDS measurements (shown below) indicate that hydrogen is completely desorbed from the surface at $T < 600\,^{\circ}$C, at least for the monohydride phase.

Figure 3 shows the peak height variation of the Ba(57 eV)MNN auger transition versus Ba deposition time on clean and on hydrogenated Si surfaces. The Ba Auger peak height increases with the coverage and the curve forms breaks joining linear parts with different

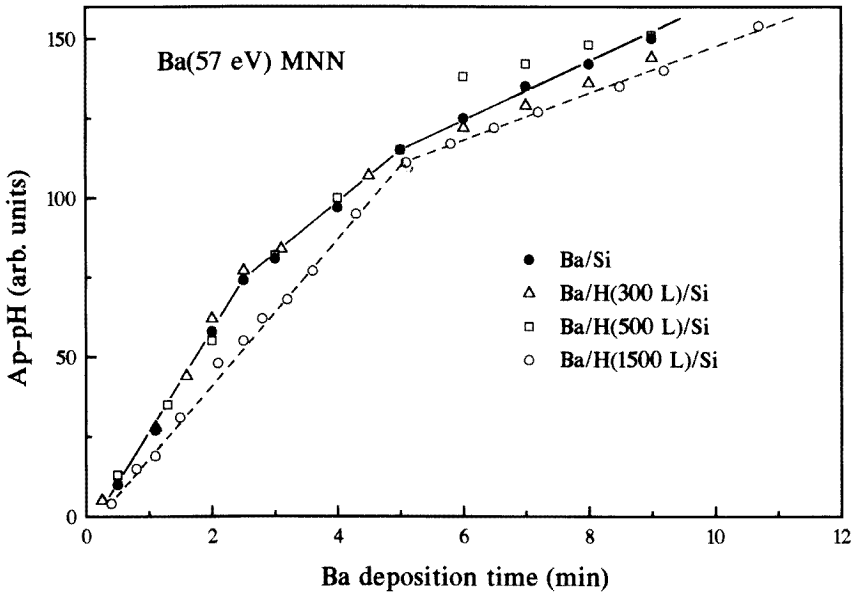

Figure 3. Ba(57 eV)MNN Auger peak height variation versus Ba deposition time on different hydrogenated Si surfaces.

slopes. The above variation of the Auger curve (As-t curve) is characteristic of a layer by layer growth (FM mode) of Ba on clean and hydrogenated Si(100) surfaces. It is obvious that the quantity of the preadsorbed H does not change the As-t curve of Ba at least for less than 1500 L H_2 exposure. From this observation, we conclude that the sticking coefficient of Ba on Si(100) remains almost constant independent of H predeposition. A similar result has been reported for K deposition on Si(100)2×1 [8]. For $\geqslant$ 1500 L H_2 the initial slope of the Ba As-t curve becomes smaller than that for a lower amount of H_2. Moreover the first break of the curve does not exist. As we will see below, we strongly believe that these two significant differences are due to the different structure of the hydrogen saturated silicon surface.

As mentioned earlier, Ba adsorption on clean Si causes a disordering of the surface due to the strong Ba–Si interaction [34]. On the other hand, when Ba adsorption takes place on either hydride phase, the substrate structure does not change substantially before the Ba coverage reaches 1.5 ML. Probably the preadsorption of H on the surface prevents the strong interaction between the Ba and Si surface atoms which causes the surface disordering. The premonolayer break which is formed at 0.5 ML for both clean and monohydrogenated Si(100) does not appear for Ba adsorption on the dihydride phase (curve of 1500 L). Therefore the premonolayer break is characteristic only for the (2×1) substrate symmetry. In the case of clean Si(100)2×1 and monohydride phase, there are adsorption sites with different symmetry such as pedestal, cave, and valley bridge sites (figure 4). Most likely the Ba atoms are initially adsorbed only on the raised pedestal sites giving an intense Auger peak height (Ap-pH) increase up to 0.5 ML. Further Ba adsorption induces the filling of different sites, specifically the more open adsorption sites, either cave or valley bridge sites. In these sites Ba adatoms are slightly submerged into the Si surface, resulting in a lower rate of Ap-pH increase above 0.5 ML and the formation of the premonolayer break. So

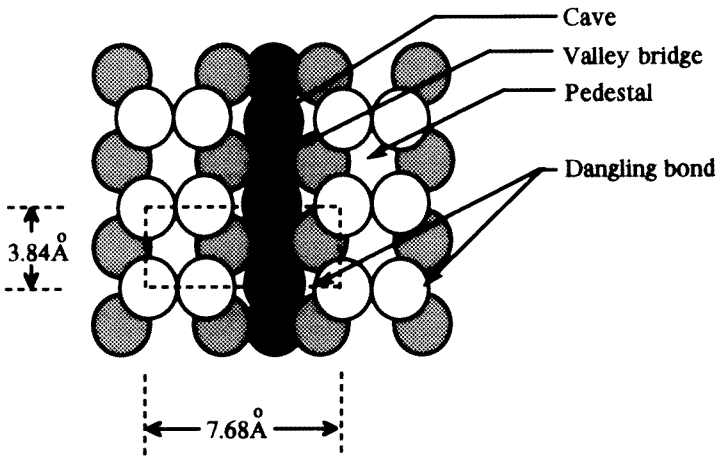

Figure 4. A top view of the Si(100)2 × 1 surface showing different adsorption sites. The 2 × 1 unit cell is indicated by dashed lines. A darker circle represents a dipped silicon atom in the bulk.

the arrangement of the first monolayer of Ba on the monohydrided Si surface supports the double-layer (DL) model proposed by Abukawa and Kono [61]. In contrast, for the dihydride phase, which shows a (1×1) symmetry, the premonolayer break does not appear because all the adsorption sites are symmetric and equivalent. This symmetry gives a constant rate of the Ba Auger signal increase up to 1 ML. During Ba adsorption on dihydride phase, the position of Ba atom is deeper because no raised pedestal sites exist any longer on the Si surface. This is the reason why the initial slope of the Ba As-t curve is smaller. According to the above discussion, simplified possible adsorption models of Ba on both hydrogenated Si surfaces are shown in figures 5 and 6. The site assignment for Ba is consistent with the DL model.

The WF variation versus the Ba deposition time on clean and various hydrogenated Si(100) surfaces is shown in figure 7. The general shape of the WF curves with and without hydrogen is almost the same. However, we can observe changes in the initial slope, the position of the WF minimum (Φ_{min}), and the final WF value (Φ_f). The initial slope is proportional to the initial electric dipole moment of the adatoms. It is well known that this WF reduction is due to some charge transfer from the adsorbate to substrate, polarizing the adatom positively [62]. In this process each Ba atom produces a surface dipole moment p, which at the early deposition stage is given by the Helmholtz equation

$$p_0 = -(4\pi 300 \times 10^{-18})^{-1}(\Delta\Phi/\Delta n)_{n\to 0} \tag{2}$$

where Δn is the number of adatoms which causes the work function change $\Delta\Phi$. The initial electric dipole moment p_0 is in Debye units. Table 2 shows the variation of p_0 and the shift of the WF minimum towards higher barium coverage with increasing predeposited hydrogen quantity on the silicon surface. It also shows the variation of the final WF value, which is denoted by Φ_f. The absolute WF value of silicon has been considered to be $\Phi_{Si} = 4.7$ eV [63]. Using this value, we transform the work function change $\Delta\Phi_i$ into absolute WF value Φ_i, by the following equation:

$$\Phi_i = \Phi_{Si} + \Delta\Phi_i. \tag{3}$$

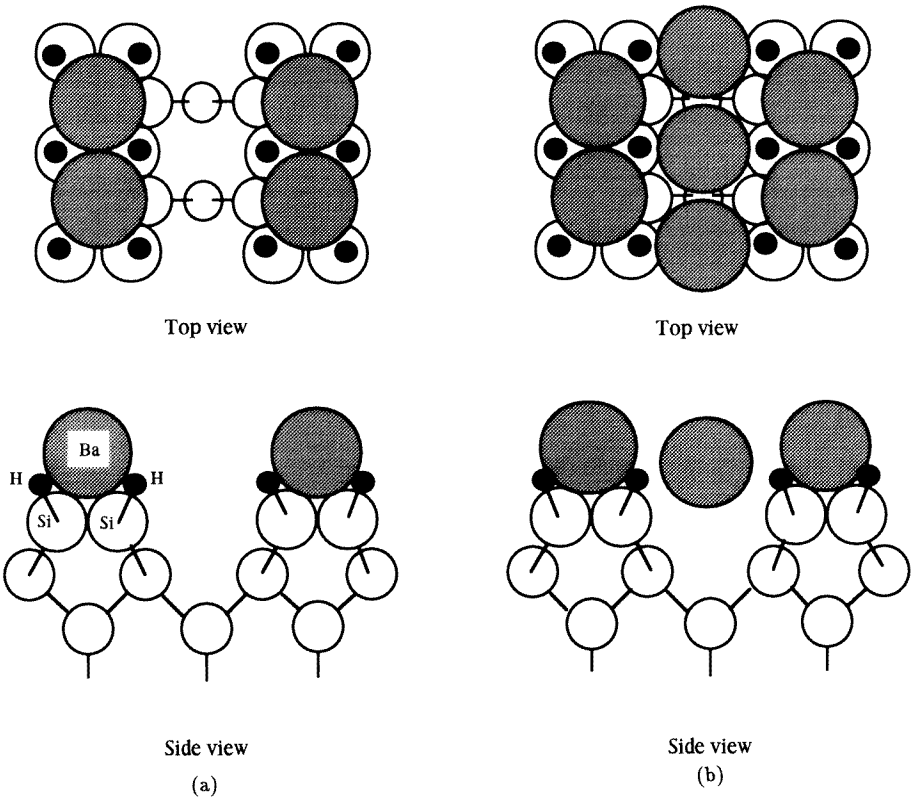

Figure 5. A schematic view of the proposed simplified model for Ba adsorption on the monohydrogenated Si(100)2 × 1 surface. (a) Ba(0.5 ML)/Si(100)2 × 1:H, top and side views; (b) Ba(1 ML/Si(100)2 × 1:H, top and side views. In the scheme cave sites are filled. The model with valley bridge sites occupied is also not excluded. All the atoms are represented by their atomic radii, except Ba atoms which are drawn by half of the ionic plus covalent radius sum.

This is mainly done for simplicity reasons.

The preexistence of hydrogen in the monohydride phase causes a small increase of the initial dipole moment p_0 of about 15–25% as compared to that of clean silicon. According to the theory of Muscat and Batra [12], this increase may be due to the longer interatomic distance between barium and silicon atoms because of the hydrogen interposition. Potassium adsorption on hydrogenated Si(100) has shown the same behaviour [8]. Also, alkali metal adsorption on several hydrogenated metallic surfaces results in a greater dipole moment p_0 [9–11]. In these cases the hydrogen interlayer has been considered quite inert. In our case, as we will see below, an interaction between Ba and H atoms with a rather ionic character cannot be excluded. When the Ba adsorption takes place on the (1×1) dihydride structure, the dipole moment decreases about 30%. In this case most of the pedestal adsorption sites have been transformed into symmetric and equivalent sites resulting a decrease in dipole length with consequent smaller p_0. This is consistent with our simplified proposed model in figure 6 where the Ba adatoms are relaxed deeper on the ideal (1×1) Si surface.

Another remarkable report in table 2 is that the absolute value of Φ_{min} decreases and is shifted to greater Ba coverage as the H concentration increases on the surface up to

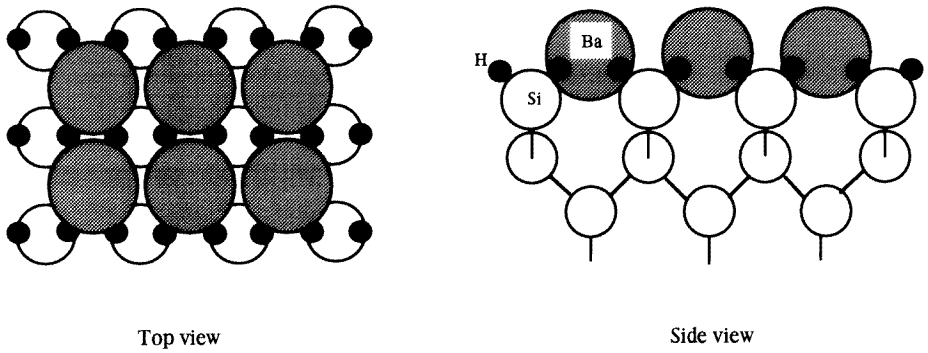

Figure 6. A schematic view of the proposed model for Ba adsorption on the dihydrided Si(100)2 × 1 surface. Both top and side views are shown for Ba(1 ML)/Si(100)1 × 1::2H.

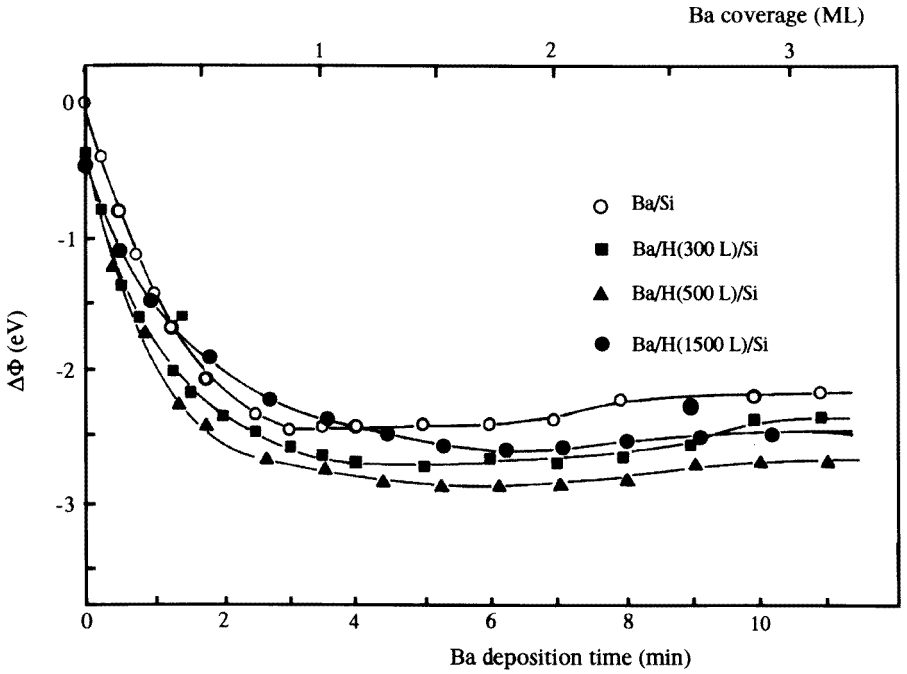

Figure 7. Work function variation $\Delta\Phi$ versus Ba deposition time for clean and various hydrogenated silicon surfaces.

completion of the monohydride phase. The lowering of the WF minimum is consistent with the dipole moment increase. However, Φ_{min} increases for Ba deposition on the dihydride phase. This may be due to the lower dipole moment resulting from the new surface symmetry (1 × 1). The shift of Φ_{min} to higher Ba coverage can be attributed to a delay in the metallization of the Ba layer with increasing H coverage. These results do not agree with those of alkali and H coadsorption [8–11]. According to these reports, preadsorption of H causes an early metallization near the completion of the first layer [8–11]. The delay of metallization of Ba is rather strange. Ba has high electron density as

Table 2.

Substrate	Φ_{min} (±0.05 eV)	Θ of Φ_{min} (ML)	p_0 (Debye)	Φ_f (±0.05 eV)
Clean Si(100)	2.25	0.8	2.35	2.50
H(300L)/Si(100)	1.95	1.2	2.75	2.30
H(500L)/Si(100)	1.80	1.5	2.90	1.95
H(1500L)/Si(100)	2.05	1.8	1.70	2.20

compared to other alkali metals (K, Cs, etc), because of the full 6s atomic orbital. Such a factor should enhance the metallization of the Ba overlayer. A possible explanation could be an interaction between Ba and H which weakens the Ba–Ba interaction, thus preventing the metallic condensation for $\Theta \leqslant 2$ ML. The changes of the Φ_f with H_2 preadsorption follow the variations of the Φ_{min}. For the dihydride phase, substrate structure is restored and the nature of the Ba–H interaction may be different, resulting in a relatively greater final WF than those on monohydride.

Figure 8 shows TD spectra of Ba on clean and H covered Si(100)2×1 surfaces. These spectra show the development of two peaks, a high-temperature peak at about 930 °C and a second one at lower temperature, 375 °C. It appears that the presence of hydrogen does not change the relative position of the two peaks. The explanation of these peaks has been given in a recent report of Ba on clean Si(100)2×1 [34]. Briefly the low-energy peak is associated with the metallic character of Ba overlayers for $\Theta > 2$ ML, while the high-energy peak is due to the relatively strong direct interaction between Ba and Si substrate. The total area under the spectra of the same Ba dosage on clean and hydrogenated Si is about the same, indicating that the Ba coverage is independent of predeposited hydrogen. This is consistent with the constant sticking coefficient of Ba on clean and hydrogenated surfaces (figure 3). However, the presence of H makes the low-energy peak smaller and the high-energy peak higher than those of Ba on clean Si(100)2×1. This is in agreement with the view which has been supported by the WF measurements, that the preadsorbed H delays the metallization of the Ba overlayer.

The TDS measurements of H_2 signal after several Ba doses are presented in figure 9. The spectrum of monohydride phase of 400 L hydrogen on clean Si(100)2×1 has only a single peak at about 510 °C, which is related to β_1 monohydride state. Deposition of half a Ba monolayer on the above hydrogenated Si surface causes a significant decrease of this H_2 TD peak (nearly 50%). This may imply that Ba adatoms remove some of the H atoms, probably one of the two H atoms bound on each dimer. The fact that the desorption energy of Ba for $\Theta < 2$ ML (the high-temperature peak in figure 8) is greater than that of H on clean Si (figure 2) means that Ba–Si interaction is stronger than that of Si–H, which is consistent with the removal of H. Further Ba deposition does not induce any substantial H_2 desorption. Instead, it causes the formation of a new H adsorption state β_3 with lower binding energy at a temperature of about 425 °C. A similar decrease of H_2 desorption peak has been also observed for K adsorption on H/Si(100), but without the formation of a new H energy state [19]. This shift of H to lower binding energy is probably due to the weakening of the Si–H bond in the presence of Ba adatoms in the Si caves or valley sites for $\Theta > 0.5$ ML. This may happen because of the charge transfer between Ba and Si atoms. Using the known Redhead equation (1) we calculate the desorption energy of the H atom in this energy state as $E = 207.6$ kJ mol^{-1} or 2.14 eV/atom. With increasing Ba coverage, the new H_2 TD peak also increases. For Ba coverage higher than 3 ML, the TD hydrogen peaks do not change. In this adsorption stage the Ba overlayer becomes rather metallic and the Ba–Ba

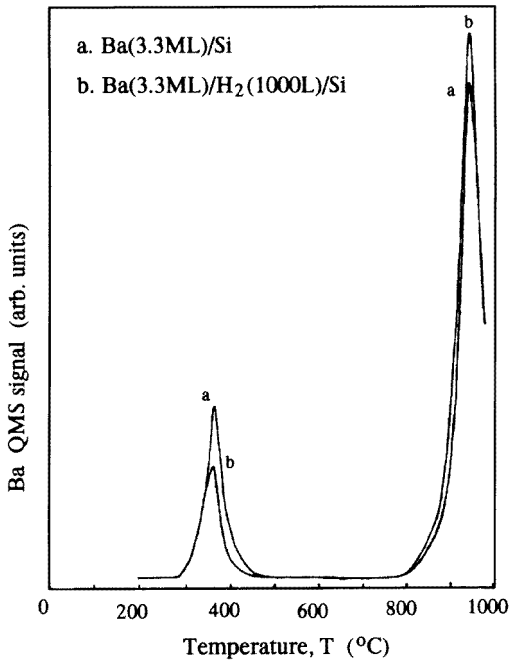

Figure 8. TD curves of Ba for Ba deposition on clean and hydrogenated Si(100)2 × 1.

interaction dominates without any further effect on the H atoms.

TDS measurements of H_2 for Ba adsorption on the saturated dihydride phase Si(100)1 × 1::2H are shown in figure 10. Upon Ba adsorption to 1 ML, both TD peaks β_1 and β_2 decrease, while two new peaks appear, one at a relatively low temperature of about 220 °C which is denoted the β_4 peak, and a second one β_5 at higher temperature near 680 °C. These two peaks appear only for the Ba adsorption on the dihydride phase. The presence of Ba weakens the binding energy of the H in the dihydride phase resulting in a partial H desorption at low temperature (β_4 peak). The desorption energy of this state has been calculated by the Redhead equation at about $E = 146.5$ kJ mol^{-1} or 1.51 eV/atom. For this calculation we used the same preexponential frequency factor $\nu_2 = 3 \times 10^{15}$ s^{-1} as we did in the case of the dihydride phase on clean Si. This desorption energy is close to the enthalpy of BaH_2 formation, $\Delta H = -171.2$ kJ mol^{-1} [64], which may imply the formation of BaH_2 on the surface close to 1 ML Ba deposition on dihydride species. As the Ba concentration increases above 1 ML the ratio of Ba to H atoms also increases, inducing the higher desorption β_3 and β_5 energy states of hydrogen. These new hydrogen states are developed as the hydrogen coverage increases up to 3 ML. With increasing Ba coverage, the height of the β_1 peak decreases while that of β_3 increases as in the case of figure 9. Meanwhile, Ba interacts with some of the preadsorbed H in the dihydride phase producing a ternary Ba–H–Si complex, of which H is strongly bound giving the β_5 desorption peak. Similar indications about Ba hydride formation have been carried out for Ba evaporation on hydrogenated Pd surfaces [16]. In the latter case it is not possible to distinguish between Ba hydride and a ternary Ba–H–Pd alloy. Moreover some other works on K and H codeposition on metallic substrates have led to similar conclusions [13, 18].

We did not detect any Ba hydride compound by QMS. We also did not observe any Ba TD peak at the temperatures of the β_4, β_3 and β_5 peaks. In other words Ba does not desorb

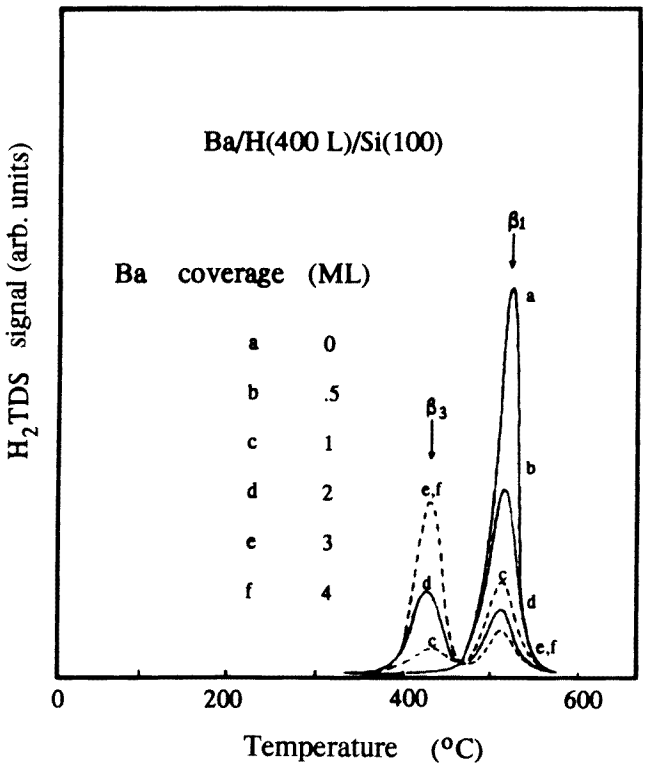

Figure 9. TD curves of H_2 for several Ba coverages on monohydrogenated Si(100)2 × 1.

as any Ba–H compound.

Figure 11 shows the EELS measurements for Ba adsorption on the monohydrogenated Si(100)2 × 1 surface. Clean silicon shows two loss peaks at 12.3 and 18.3 eV. The first peak has been assigned to the silicon surface plasmon and the second one to the corresponding bulk plasmon. Hydrogen adsorption on the clean Si causes the appearance of a new peak at about 10 eV. This peak is probably due to the Si–H interaction during the monohydride phase. Ibach and Rowe [35] have identified a similar peak at 8.5 ± 1 eV, attributing this peak to the transition from the state of the H–Si bond. Upon Ba(0.5 ML) adsorption two new loss peaks appear at 11.7 and 25.3 ± 0.5 eV. In the case of Ba on clean Si a loss peak appears at about 11 eV, which has been attributed to a $5p_{3/2}$ to 6s electronic transition due to the strong Ba–Si interaction [34]. This loss peak shifts by 0.7 eV to higher energy with H preadsorption. This is probably due do the partial interaction between Ba and H atoms on the dimers. As Ba coverage increases this loss peak moves slightly towards lower energy, approaching the value of 11 eV. This may happen because as Ba occupies valley or cave sites it interacts more directly with the Si atoms. AT 3 ML Ba coverage this peak has almost disappeared. This is reasonable because the ionicity of Ba adatoms decreases for $\Theta > 2$ ML where Ba metallization starts. On the other hand the loss peak at 25.3 eV has been assigned to another electronic transition from 5p to 4f (or 5d) [65]. The intensity of this peak decreases also for $\Theta > 2$ ML. Above this coverage metallization starts, making 5p, 4f, and 5d states less localized because of the hybridization between Ba adatoms. On

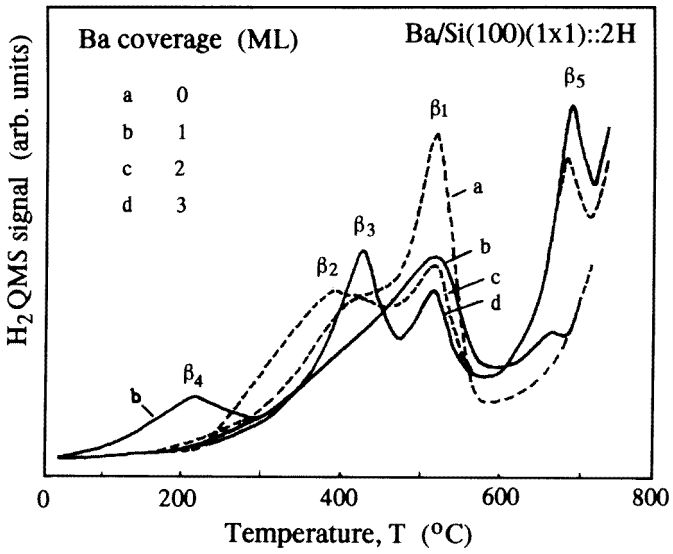

Figure 10. TD curves of H_2 for several Ba coverages on dihydrogenated Si(100)2 × 1.

the other hand, the bulk plasmon peak disappears completely due to the masking effect of the Ba overlayer. EELS results also obtained for the dihydride phase (not shown) are quite similar.

4. Conclusions

In this study, we investigate Ba and H coadsorption on Si(100)2 × 1 by AES, TDS, LEED, EELS, and WF measurements.

Hydrogen adsorption on clean Si(100)2 × 1 was carried out for reference purposes confirming earlier results. Two different hydrogen phases are formed, known as monohydride phase Si(100)2 × 1: H and dihydride phase Si(100)1 × 1: : 2H.

Barium deposition took place on the above hydrogen phases. The DL model seems to be applied for a Ba array on the monohydride phase. Ba adatoms first occupy pedestal sites and consequently caves or valley bridge sites in the surface troughs between dimer rows. In this way the (2 × 1) structure remains up to $\Theta = 1$ ML. When adsorption of Ba takes place on the dihydride phase, the Ba adatoms are relaxed at symmetric and equivalent sites following the (1 × 1) symmetry of the restored Si surface for coverage $\Theta = 1$ ML. Further Ba adsorption leads to all surface disordering. The sticking coefficient of Ba remains almost constant independent of the preadsorbed H quantity. Ba on clean Si becomes metallic for $\Theta > 2$ ML. the presence of preadsorbed H causes a delay of the Ba overlayer metallization, which depends on the amount of preadsorbed H. This is in contrast to the case of early metallization of alkali (K and Cs) overlayers on the hydrogenated Si(100)2 × 1 surface. This probably happens because of the interaction of Ba with the H on the Si(100) substrate. TD measurements indicated that during the initial Ba adsorption on monohydrided silicon surface some of the H atoms desorb from the surface. As Ba coverage increases, the Ba on the monohydride phase weakens the Si–H binding. In the case of Ba on dihydride phase, in the early stage of adsorption, Ba interacts also with H, probably forming a BaH_2 hydride.

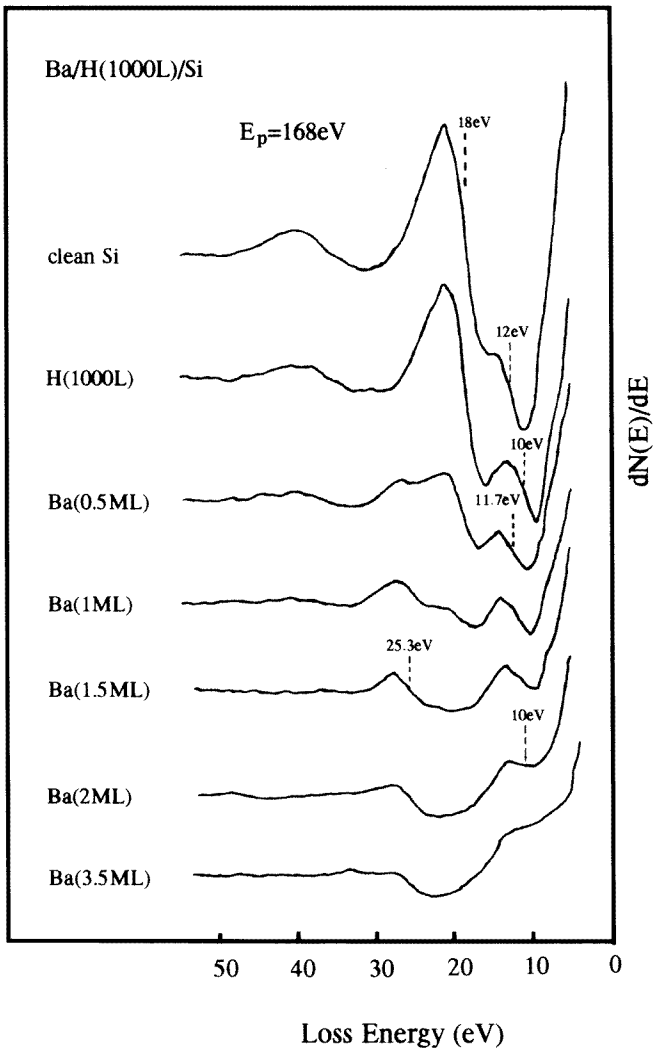

Figure 11. EELS spectra for several Ba coverages on hydrogenated Si(100)2 × 1.

With further Ba coverage increase above 1 ML the Ba to H atom ratio changes and the latter hydride is transformed into a higher-energy binding state which probably corresponds to a complex ternary Ba–H–Si compound. Above 3 ML, the Ba–Ba interaction dominates, resulting in the metallization of the Ba overlayer.

Acknowledgment

We wish to thank Dr M Kamaratos for his help during the experiment and his useful suggestions.

References

[1] Rhead G E 1991 *Appl. Surf. Sci.* **52** 19 and references therein
[2] Ertl G, Lee S B and Weiss M 1982 *Surf. Sci.* **114** 527
[3] Heskett D, Strathy I, Plummer E W and de Paola R A 1985 *Phys. Rev.* B **32** 6222
[4] Hatsopoulos G N and Gyftopoulos E P 1979 *Thermionic Conversion* (Cambridge, MA: MIT)
[5] Spicer W E 1977 *Appl. Phys.* **12** 115
[6] Edwards D and Perria W T 1979 *Appl. Surf. Sci.* **1** 419
[7] Bonzel H P, Bradshaw A M and Ertl G 1989 *Physics and Chemistry of Alkali Metal Adsorption* (Amsterdam: Elsevier)
[8] Papageorgopoulos C A and Kamaratos M 1990 *Vacuum* **41** 567
[9] Papageorgopoulos C A 1989 *Phys. Rev.* B **40** 1546
[10] Ernst-Vidalis M L, Kamaratos M and Papageorgopoulos C A 1987 *Surf. Sci.* **189/190** 276
[11] Papageorgopoulos C A and Chen J M 1973 *Surf. Sci.* **39** 283
[12] Muscat J P and Batra I 1986 *Phys. Rev.* B **34** 2889
[13] Paul J and Hoffmann F M 1988 *Surf. Sci.* **194** 419
[14] Paul J and Hoffmann F M 1988 *Proc. 9th Int. Congr. on Catalysis (Calgary, 1988)* p 1890
[15] Lanzillotto A M, Dresser M J, Alvey M D and Yates J T 1988 *J. Chem. Phys.* **89** 570
[16] Fischer A, Krozer A and Schlapbach L 1992 *Surf. Sci.* **269/270** 737
[17] Johnson P D, Viescas A J, Nordlander P and Tully J C 1990 *Phys. Rev. Lett.* **64** 942
[18] Schmid L D and Gomer R 1965 *J. Chem. Phys.* **43** 95
[19] Takagi N, Minami N and Nishijima M 1992 *Phys. Rev.* B **45** 13 524
[20] Souzis A E, Seidl M, Carr W E and Huang H 1989 *J. Vac. Sci. Technol.* A **7** 720
[21] Yasue T and Ichimiya A 1990 *Vacuum* **41** 567
[22] Nishijima M, Tanaka S, Takagi N and Onchi M 1991 *Surf. Sci.* **242** 498
[23] van Bommel P J M, Geerlings J J C, van Wunnic J N M, Massmann P, Granneman E H A and Los J 1983 *J. Appl. Phys.* **54** 5676
[24] Pargellis A and Seidl M 1982 *Phys. Rev.* B **25** 4356
[25] Seidl M and Pargellis A 1982 *Phys. Rev.* B **26** 1
[26] van Os C F A, van Amersfoort P W and Los J 1988 *J. Appl. Phys.* **64** 3863
[27] van Os C F A, Leguijt C, Heeren R M A, Los J and Kleyn A W 1989 *SPIE* vol 1061 (Bellingham, WA: SPIE) 568–72
[28] van Os Ron 1989 *PhD Thesis* Utrecht
[29] Heeren R M A, Ciric D, Yagura S, Hapman H J and Kleyn A W 1992 *Nucl. Instrum. Methods* B **69** 389
[30] Mueller W M, Blackedge J P and Libowitz G G 1968 *Metal Hydrides* (New York: Academic)
[31] Schaplbach L Hydrogen in Intermetallic Compounds II (*Topics in Applied Physics 64*) ed L Schlapbach (Berlin: Springer) ch 2
[32] Yu R and Lam P K 1988 *Phys. Rev.* B **37** 8730
[33] Wu J Y, Trickey S B and Boetteger J C 1990 *Phys. Rev.* B **42** 1663
[34] Vlachos D, Kamaratos M and Papageorgopoulos C 1994 *Solid State Commun.* **90** 175
[35] Ibach H and Rowe J E 1974 *Surf. Sci.* **43** 481
[36] Ciraci S, Butz R, Oelling E M and Wagner H 1984 *Phys. Rev.* B **30** 711
[37] Sakurai T and Hagstrum H D 1976 *Phys. Rev.* B **14** 1593
[38] White S J, Woodruff D P, Holland B W and Zimmer R S 1978 *Surf. Sci.* **74** 34
[39] Koke P and Mönch W 1980 *Solid State Commun.* **36** 1007
[40] Stucki F, Schaefer J A, Anderson J R, Lapeyre G J and Gopel W 1983 *Solid State Commun.* **47** 795
[41] Madden H H 1981 *Surf. Sci.* **105** 129
[42] Maruno S, Iwasaki H, Horioka K, Li S T and Nakamura S 1983 *Phys. Rev.* B **27** 4110
[43] Chabal Y J and Ragharachari K 1985 *Phys. Rev. Lett.* **54** 1055
[44] Gupta P, Colvin V L and George S M 1988 *Phys. Rev.* B **37** 8234
[45] Flowers M C, Jonathan N B H, Liu Y and Morris A 1993 *J. Chem. Phys.* **99** 7038
[46] Boland J J 1990 *Phys. Rev. Lett.* **65** 3325
[47] Mortensen K, Chen D M, Bedrossian P J, Golovchenko J A and Besenbacher F 1991 *Phys. Rev.* B **43** 1816
[48] Batra I P, Ciraci S and Ortenburger I B 1976 *Solid State Commun.* **18** 563
[49] Appelbaum J A and Hamann D R 1977 *Phys. Rev.* B **15** 2006
[50] Wu C J and Carter E A 1991 *Chem. Phys. Lett.* **185** 172
[51] Nachtigall P, Jordan K D and Janda K C 1991 *J. Chem. Phys.* **95** 8652
[52] Uchiyama T and Tsukada M 1993 *Surf. Sci. Lett.* **295** L1037

[53] Wu C J, Ionova I V and Carter E A 1993 *Surf. Sci.* **295** 64
[54] Jing Z and Whitten J L 1993 *J. Chem. Phys.* **98** 7466
[55] Uchuiyama T and Tsukada M 1994 *Surf. Sci.* **313** 17
[56] Chadi D J 1979 *J. Vac. Sci. Technol.* **16** 1290; 1979 *Phys. Rev. Lett.* **43** 43
[57] Sinniah K, Sherman M G, Lewis L B, Weinberg W H, Yates J T Jr and Ianda K C 1989 *Phys. Rev. Lett.* **62** 567
[58] Suemitsu M, Nakazawa H and Miyamoto N 1994 *Appl. Surf. Sci.* **82/83** 449
[59] Redhead P A 1962 *Vacuum* **12** 203
[60] Hofer U, Li L and Heinz T F 1992 *Phys. Rev.* B **45** 9485
[61] Abukawa T and Kono S 1988 *Phys. Rev.* B **37** 9097
[62] Langmuir I and Taylor J B 1932 *Phys. Rev. Lett.* **31** 102
[63] Fainstein S M 1968 *Zavodskaya Lab.* **14** 64
[64] 1952 *Circular of the National Bureau of Standards* 500
[65] Dowben P A and Lagraffe D 1990 *Phys. Lett.* **144A** 193